Title: Controls on millennial-scale atmospheric CO_2 variability during the last glacial period

Authors:
Bauska, T.K.[1,2]*, Brook, E.J.[2], Marcott, S.A.[3], Baggenstos, D.[4], Shackleton, S.[4], Severinghaus, J.P.[4], Petrenko, V.V.[5]

1: Godwin Laboratory for Palaeoclimate Research, Department of Earth Sciences, University of Cambridge, Downing Street, CB2 3EQ, United Kingdom

2: College of Earth, Ocean, and Atmospheric Sciences, Oregon State University, 104 CEOAS Admin Bldg, Corvallis, OR 97331, USA

3: Department of Geoscience, University of Wisconsin-Madison, 1215 W Dayton St. Madison, WI 53706, USA

4: Scripps Institution of Oceanography (SIO), University of California, San Diego, La Jolla, CA, 92093, USA.

5: Department of Earth and Environmental Sciences, University of Rochester, Rochester, NY 14627, USA

*tkb28@cam.ac.uk

Key points

- A new ice core record of the stable isotopes of atmospheric CO_2 suggests organic carbon sources controlled CO_2 levels during the last glacial period
- The millennial-scale CO_2 variability is tentatively linked to variations in Southern Ocean carbon sources
- Centennial-scale CO_2 variability during the last glacial period is associated with similarly abrupt changes during the deglaciation

Abstract

Changes in atmospheric CO_2 on millennial-to-centennial timescales are key components of past climate variability during the last glacial and deglacial periods (70-10ka) yet the sources and mechanisms responsible for the CO_2 fluctuations remain largely obscure. Here we report the $^{13}C/^{12}C$ ratio of atmospheric CO_2 during a key interval of the last glacial period at sub-millennial resolution, with coeval histories of atmospheric CO_2, CH_4 and N_2O concentrations. The carbon isotope data suggest that the millennial-scale CO_2 variability in MIS3 is driven largely by changes in the organic carbon cycle, most likely by sequestration of respired carbon in the deep ocean. Centennial-scale CO_2 variations, distinguished by carbon isotope signatures, are associated with both abrupt hydrological change in the tropics (e.g. Heinrich Events) and rapid increases in northern hemisphere temperature (DO events). These events can be linked to modes of variability during the last deglaciation, thus suggesting that drivers of millennial and centennial CO_2 variability during both periods are intimately linked to abrupt climate variability.

Plain Language Summary

Ice cores provide unique records of variations in atmospheric CO_2 prior to the instrumental era. While it is clear that changes in atmospheric CO_2 played a significant role in driving past climate change, it is unclear what in turn drove changes in atmospheric CO_2. Here we investigate enigmatic changes in atmospheric CO_2 levels during an interval of the last glacial period (~50,000 to 35,000 years ago) that are associated with abrupt changes in polar climate. To determine the sources and sinks for atmospheric CO_2 we measured the stable isotopes of carbon in CO_2 and found that the primary source of carbon to the atmosphere was an organic carbon reservoir. Most likely, this carbon was sourced from a deep ocean reservoir that waxed and waned following changes in either the productivity of the surface ocean or stratification of the deep ocean. We also found that atmospheric CO_2 can change on the centennial time-scale during abrupt climate transitions in the Northern Hemisphere. This observation adds to a growing body of evidence that abrupt changes in atmospheric CO_2 are an important component of past carbon cycle variability.

Introduction

In order to predict the climate impacts of anthropogenic CO_2 emissions over the coming millennia (Clark et al., 2016) we must understand how the climate system and carbon cycle have interacted over these same timescales in the past. The CO_2 rise during the last deglaciation, arguably the most well-studied example of past carbon cycle variability, is likely a combination of millennial-scale climate change and glacial-interglacial shifts in temperature and ice volume, which are all amplified through a system of climate-carbon cycle feedbacks. To disentangle the millennial-scale component we investigate carbon cycle variability of the last glacial period when climate variations were largely unaffected by changes in northern hemisphere insolation and ice volume that characterize glacial terminations (Figure S1).

During Marine Isotope Stage 3 (MIS3) atmospheric CO_2 varied between about 195 and 225 ppm with a roughly triangular waveform (Indermühle, 2000) (Figure 1 E). This pattern mimics Antarctic temperature, rising during the strongest Antarctic warmings and falling during the coolings (Figure 1 B). From the perspective of Greenland climate and the well-known Dansgaard-Oeschger events (DO), CO_2 increases during cold phases (stadials)(Ahn & Brook, 2008) with the most prominent increases corresponding to only those stadials associated with an enhanced flux of debris-laden ice to the North Atlantic (known as a Heinrich Events; these specific cold intervals are often referred to as "Heinrich stadials"). CO_2 decreases after a rapid switch to warmer conditions over Greenland (interstadials) and slower cooling in Antarctica (Bereiter et al., 2012). This strong relationship between Antarctic temperature and CO_2 has focused attention on the Southern Ocean (SO) as the major conduit for the transfer of carbon between the atmosphere and the ocean on millennial and glacial-interglacial timescales (Sigman et al., 2010), with possible triggers in the North Atlantic.

The ratios of carbon isotopes differ among key carbon reservoirs and thus some of the sources and sinks driving past atmospheric CO_2 can be constrained using the isotopic composition of atmospheric CO_2 (Bauska et al., 2016; Schmitt et al., 2012; Köhler et al., 2006; Eggleston et al., 2016). Four major processes fractionate the carbon isotopes ($\varepsilon_{A\text{-}B} \sim= \delta^{13}C_A - \delta^{13}C_B$): photosynthesis that makes CO_2 into organic carbon on land ($\varepsilon_{land\text{-}atmosphere} = \sim$-18‰), photosynthesis in the surface ocean that forms particulate organic carbon from dissolved inorganic carbon ($\varepsilon_{DIC\text{-}POC} = \sim$-22‰), air-sea gas exchange ($\varepsilon_{DIC\text{-}atmosphere} = +\sim$8‰; decreasing by 0.1‰ for every 1°C increase in ocean temperature), and a negligible fractionation during the formation of $CaCO_3$ in surface ocean, ($\varepsilon_{DIC\text{-}CaCO3} = \sim$0‰). By measuring the time varying changes in both atmospheric CO_2 concentrations and the $\delta^{13}C$ isotopes, we can constrain the sources of the CO_2 changes. Rising atmospheric CO_2 and decreasing $\delta^{13}C\text{-}CO_2$ is consistent with organic carbon sources to the atmosphere; rising atmospheric CO_2 and increasing $\delta^{13}C\text{-}CO_2$ is consistent with a warming ocean; and rising CO_2 with no changes in $\delta^{13}C\text{-}CO_2$ could indicate a balanced contribution of rising ocean temperature and organic carbon sources or the influence of

$CaCO_3$ or volcanic sources. Air-sea gas exchange in the high-latitude ocean may affect atmospheric $\delta^{13}C\text{-}CO_2$, with rising atmospheric CO_2 and large decreases in $\delta^{13}C\text{-}CO_2$ predicted by box model experiments that include enhanced air-sea gas exchange in the SO(Bauska et al., 2016; Köhler et al., 2006). Finally, changes in the abundance of C3 and C4 plants on land (Ehleringer et al., 1997) or ecological shifts in marine biosphere (Broecker & McGee, 2013) would change the overall photosynthetic fractionation and thus the details, but not the fundamentals, of using $\delta^{13}C\text{-}CO_2$ to fingerprint carbon sources.

Other atmospheric gases provide additional constraints on carbon cycle variability, particularly related to the response of the terrestrial biosphere to abrupt climate change. Most evidence suggests that past variations in methane are dominated by climate variability over tropical and boreal wetlands (Brook et al., 2000; Rhodes et al., 2015). N_2O is produced in oxygen-poor ocean waters and terrestrial soils. Rising N_2O most likely reflects either decreasing oxygen levels in the intermediate-depth ocean, warmer terrestrial soil temperatures or a combination of the two (Schilt et al., 2014). The $\delta^{18}O\text{-}O_2$ largely follows the changes in $\delta^{18}O$ of seawater and orbitally-driven changes in the Dole effect, but rapid increases in $\delta^{18}O\text{-}O_2$ have been argued to reflect southward shifts in low-latitude precipitation (Seltzer et al., 2017; Severinghaus et al., 2009) (see SI for definition of $\Delta\varepsilon_{LAND}$).

Methods and Materials

We present new atmospheric histories of CO_2, N_2O, CH_4 and $\delta^{13}C\text{-}CO_2$ spanning 47-35 ka from the Taylor Glacier, Antarctica blue ice area (Figure 1 D-G). The chronology (Baggenstos et al., 2017) is constructed by synchronizing the Taylor Glacier CH_4 and $\delta^{18}O\text{-}O_2$ records to the WDC timescale (Buizert et al., 2015) and thus linking to the radiometrically dated Hulu Cave record (Cheng et al., 2016) (Figure 1 C). The concentrations of CO_2 and N_2O and the $\delta^{13}C\text{-}CO_2$ were measured on the same sample using the Oregon State University ice grater system (Bauska et al., 2014). The long-term reproducibly for CO_2, N_2O and $\delta^{13}C\text{-}CO_2$ are ±1ppm, ±5 ppb, +0.02‰, respectively (Bauska et al., 2015; Bauska et al., 2016). The combination of increased resolution and precision equates to a significant improvement over previous reconstructions which focused on longer-term changes (Eggleston et al., 2016) (Figure S1). Additionally, previous reconstructions in this time interval were limited by offsets between cores (see *Eggleston et al., 2016* for detailed discussion and Figure S2). Using the interval from 47 to 43ka as a baseline for comparison, the Talos Dome $\delta^{13}C\text{-}CO_2$ record has significantly lower and more variable values (mean±s.d. = -6.72±0.23‰; n = 12) than data from the EDML (-6.50±0.12‰; n = 8) and EDC (-6.59±0.16‰; n = 5) ice cores. In the same interval, the Taylor Glacier averages -6.55±0.07‰ (n = 14) in broad agreement with EDML and EDC. Although we can confidently interpret relative changes in our new record because of the improvement in precision and resolution, addressing the absolute accuracy of the $\delta^{13}C\text{-}CO_2$ values requires additional inter-laboratory and inter-core comparison.

147

148 **Results: Ice Core Constraints on Greenhouse Gas Variability**

149 The most salient mode of variability in atmospheric CO_2, the millennial-scale rising and falling with
150 Antarctic temperature, is accompanied by an inversely correlated change in $\delta^{13}C\text{-}CO_2$ (Figure 1 E-F).
151 Atmospheric CO_2 ranges from about 195 to 215 ppm with the corresponding variability in $\delta^{13}C\text{-}CO_2$
152 spanning -6.45 to -6.65‰ (a -0.1‰ change for every +10 ppm). At finer scales we observe several
153 other modes of variability. The CO_2 rise during Heinrich Stadial 4 (40.2-38.4 ka; "HS4") starts off
154 slowly, rising 3-4 ppm while $\delta^{13}C\text{-}CO_2$ decreases by ~0.05‰. As noted previously in the Siple Dome ice
155 core (Ahn & Brook, 2014), the rise then accelerates in a sharp jump of about 8 ppm. The rapid phase of
156 the rise is coincident with the mid-stadial rise in CH_4 noted in the WAIS Divide Core (Rhodes et al.,
157 2015) (Figure 1 D, red vertical line) and the increase in $\Delta\varepsilon_{LAND}$ first observed in the Siple Dome Core
158 (Severinghaus et al., 2009) and confirmed in the WDC record(Seltzer et al., 2017) (Figure 1 H). No
159 change in N_2O is resolved in the Taylor Glacier dataset, consistent with the Talos Dome record (Schilt
160 et al., 2010) (Figure 1 G). The resolution of the carbon isotope measurements prevents a clear
161 fingerprinting of the source but a replicated sample clearly falls to more negative values off the more
162 gradual trend by about 0.1‰ (Figure 1 F). In the later part of the HS4, CO_2 continues to rise slowly by
163 3 ppm and $\delta^{13}C\text{-}CO_2$ decreases by another 0.1‰.
164
165 The onsets of DO interstadials are accompanied by small rises in CO_2 (Figure 1 E, dashed gray lines).
166 This variability has been noted in other cores and described as either a lagged response to Antarctic
167 temperature (Bereiter et al., 2012) or, in the case of the weaker DO events, a lagged response to
168 Greenland stadial conditions that are too short to impart a significant change in CO_2 (Ahn & Brook,
169 2014). In our record we note that atmospheric CO_2 appears to increase along with CH_4, and N_2O with
170 no discernable lead or lag. This is most prominent at DO8 when CH_4 rises by about 120 ppb, N_2O rises
171 by 35 ppb and CO_2 rises by 6 ppm (see also Figure 4 n-p). The other DO events (7,9,10) are near the
172 detection limit of our record and difficult to quantity. Across these events $\delta^{13}C\text{-}CO_2$ either increases
173 slightly (~0.08‰ at DO8) or shows no substantial change.
174
175 **Discussion: Millennial-scale carbon cycle variability**

176 The overall negative correlation between CO_2 and $\delta^{13}C\text{-}CO_2$ rules out changes in ocean temperature,
177 the $CaCO_3$ cycle, or volcanic input having a dominant role in driving millennial-scale CO_2 (Figure 2).
178 Instead, the data are consistent with changes in terrestrial carbon storage or the strength of the
179 ocean's biological pump. If terrestrial sources were dominant, whole ocean $\delta^{13}C$ would follow
180 atmospheric $\delta^{13}C\text{-}CO_2$. If oceanic sources from changes in the strength of the biological pump or shifts
181 in ocean ventilation were dominant, the surface-to-deep gradient in $\delta^{13}C$ in inorganic carbon in the
182 ocean would decrease along with atmospheric $\delta^{13}C\text{-}CO_2$.
183

Millennial-scale decreases in the vertical gradient of $\delta^{13}C$ in the SO have been tentatively correlated to maxima in atmospheric CO_2 (Charles et al., 2010; Ziegler et al., 2013), and therefore in light of our new data, minima in $\delta^{13}C$-CO_2 (Figure 3a-b). If this coupling of the oceanic gradient of $\delta^{13}C$ and atmospheric $\delta^{13}C$-CO_2 could be demonstrated to be precisely in-phase it would provide clear evidence of an oceanic source controlling atmospheric CO_2. Taking the current data and chronology at face-value, the decreases in the oceanic $\delta^{13}C$ gradient are broadly associated with minima in atmospheric $\delta^{13}C$-CO_2, yet the coupling is clearly not one-to-one, possibly due to chronological errors in the marine sediment record. To explore this hypothesis further, we combined existing benthic carbon isotope records from deep SO (~42°S, 10°E, 4600 m) (Charles et al., 1996; Ninnemann et al., 1999; Hodell et al., 2001, 2003). These records use previously established age models tied to the Greenland ice core records using carbonate preservation and confirmed by ^{14}C data during the deglaciation and the Laschamp paleomagnetic event during MIS3 (~42ka) (Barker & Diz, 2014). We include a minor increase in the absolute age of 0.63% to account for the possible under-counting of annual layers in the Greenland Ice Core chronologies relative to the WAIS Divide timescale (Buizert et al., 2015).

We note that the atmosphere and deep ocean $\delta^{13}C$ are anti-correlated during MIS3 (Figure 3c). This supports the hypothesis that the waxing and waning of respired organic carbon source in the deep SO controlled atmospheric CO_2 and significantly limits the possibility of contributions from terrestrial sources. However, this relationship alone cannot delineate oceanic sources between changes in export productivity and changes in stratification. Evidence to support changes in export productivity comes from the correlation of the ice core data and foraminifera-bound $\delta^{15}N$ which indicates lower nitrate utilization during periods of high atmospheric CO_2 (Martínez-García et al., 2014) (Figure 3d). Iron deposition rates and export production in the Subantarctic are also closely coupled, suggesting that the extent of iron limitation may have played a role in this enhanced nutrient utilization (Jaccard et al., 2016). Evidence in support of ventilation changes stems from radiocarbon constraints in the South Atlantic that are closely coupled with deep ocean oxygen levels, suggesting that both export productivity and ocean circulation were working in concert over this period (Gottschalk et al., 2016). A quantitative description of this coupling requires study with isotope enabled earth system models; however, additional insight can be gained by comparing to periods when these processes may have become uncoupled.

Our new high-resolution MIS3 data now provide a similar sequence of abrupt climate change events to contrast with the last deglaciation. First, we compare the MIS3 data to the last deglaciation utilizing a cross plot of CO_2 and $\delta^{13}C$-CO_2 (Figure 2). We see that the MIS3 data fall along the same trend observed during HS1 of the last deglaciation (~18-15.0ka) yet only span about 50% of range (note that the low $\delta^{13}C$-CO_2 values that fall off this trend are due to centennial-scale variability at ~16.3 ka). This suggests that millennial-scale CO_2 variations in MIS3 can be linked mechanistically to the more pronounced

variability during the deglaciation. As discussed in previous work, this co-variability of CO_2 and $\delta^{13}C$-CO_2 is consistent with changes in SO ventilation (Köhler et al., 2006; Menviel et al., 2015; Schmitt et al., 2012; Tschumi et al., 2011) changes in export production (particularly the SO)(Bauska et al., 2016; Menviel et al., 2012) or a weakening of the ocean's biological pump by a reduction in North Atlantic Deep-water (NADW) formation (Schmittner & Lund, 2015).

Second, we compare the two intervals in time with the GHG records plotted over 8ka intervals (Figure 4a-c). Similar patterns of millennial-scale variability in CH_4 and N_2O are observed but the changes in CO_2 appear fundamentally different. First, the CO_2 rise during HS1 is about 20 ppm greater than the rise in HS4 (or ~2x) and, second, CO_2 remains elevated after the switch to interstadial conditions during the Bølling-Allerød (BA) rather than decreasing as observed after the onset of DO8 (Figure 3 C). The $\delta^{13}C$-CO_2 follows a similar pattern. In HS1 $\delta^{13}C$-CO_2 decreases by 0.2‰ more than HS4 and stabilizes during the BA as opposed to abrupt increases observed during DO8 (Figure 4 D). What was different about the deglaciation that allowed more respired carbon into the atmosphere during HS1 than HS4 and prevented, or compensated for, a potential uptake of carbon during the BA?

During the Heinrich stadials, NADW weakens (Henry et al., 2016) and Subantarctic productivity decreases (Anderson et al., 2014; Gottschalk et al., 2016) tracking dust delivery to Antarctica (Fischer et al., 2007) (Figure 4 e, h-i). Ventilation of the SO (as inferred from radiocarbon) improves (Gottschalk et al., 2016; Skinner et al., 2010) and SO upwelling (as inferred from Antarctic productivity) increases (Anderson et al., 2009), although these changes could be more pronounced in the later part of the Heinrich stadials (Figure 4 f-g). During MIS3 all of these changes are largely symmetric around, and consistent with, the minimum in $\delta^{13}C$-CO_2 and thus plausible drivers the change in CO_2.

During the deglaciation some variables trend back towards LGM values after HS1 (NADW and SO upwelling), while others, show near permanent shifts to interglacial levels during HS1 (Subantarctic productivity, SO ventilation). This decoupling allows us to partially disentangle which processes control atmospheric CO_2. Based on relationship between the proxies and atmospheric data in MIS3, we would expect that if changes in NADW and/or SO upwelling were to control atmospheric CO_2, we would observe a large CO_2 decrease and $\delta^{13}C$-CO_2 increase in the BA. This is clearly not the case and requires either a muted response to these forcings or another source of carbon in the BA that compensated for the apparent carbon sink. Conversely, if changes in Subantarctic productivity and SO ventilation dominated the atmospheric CO_2 budget, we could expect CO_2 to remain elevated during the BA and $\delta^{13}C$-CO_2 to plateau at lower values, a scenario that is in much better agreement with the data. Thus Subantarctic productivity and SO ventilation appear to have a more consistent link with

atmospheric CO_2 in both MIS3 and the Last Deglaciation and are strong candidates for contributing significantly to glacial-interglacial CO_2 change.

Discussion: Centennial-scale carbon cycle variability

On the centennial-scale our new observations in MIS3 can be combined with recently identified variability in Last Deglaciation to suggest a ubiquitous and consistent coupling of the carbon cycle with abrupt climate change events. In Figure 4j-q we plot variability in greenhouse gases for two categories of centennial-scale events: the onset of interstadials (D08, the Bølling-Allerød and the pre-Boreal) and mid-Heinrich Stadials events (H4 and H1). The changes are plotted as anomalies and the timing is set relative to the mid-point of the rise in CH_4. Note that the Taylor Glacier chronology is synchronized with the WAIS Divide record via CH_4 and thus the phasing of the two ice cores cannot be interpreted.

The rapid 8 ppm CO_2 rise during HS4 at 39.5 ka likely shares a common origin with a similar event during the deglaciation with HS1 at 16.3 ka (Marcott et al., 2014) (Figure 4l). Both events are associated with carbon isotope minima (Figure 4m). It has been suggested that these mid-stadial events can be tied to the timing of the Heinrich Events and may represent a rapid release of terrestrial carbon to the atmosphere driven by a cooling and drying of the Northern Hemisphere (Bauska et al., 2016). The event in HS4 is consistent with a terrestrial origin as it coincides with an increase in CH_4 (Rhodes et al., 2015) (Figure 4j), which may indicate enhanced precipitation of the Southern Hemisphere tropics, and an increase in $\Delta\varepsilon_{LAND}$, which suggests decreased precipitation in the Northern Hemisphere(Seltzer et al., 2017; Severinghaus et al., 2009) (Figure 1h). Constant N_2O indicates either that changes in terrestrial soil temperatures may have been small on the global scale, thus suggesting that precipitation was the dominant driver of the terrestrial carbon loss, or that oxygen-minimum zones in intermediate ocean were relatively stable, possibly indicating the absence of a change ocean circulation across this event (Figure 4k).

The 6 ppm CO_2 rise at the onset of DO8 shares common features with the onset of the BA and Preboreal (~11.5ka) during the deglaciation (Figure 4p). All three events exhibit simultaneous increases in CO_2, CH_4 and N_2O that coincide with abrupt Northern Hemisphere warmings, continued warming or at least stable temperatures in Antarctica (WAIS Divide Project Members, 2015), and greater NADW formation (Henry et al., 2016; McManus et al., 2004) (Figure 3, vertical yellow dashed lines). The $\delta^{13}C\text{-}CO_2$ across all events is variable but shows no secular trend (Preboreal) or slight increase of ~0.08‰ (B/A and DO8) (Figure 4q). At face value, this pattern of increasing CO_2 and increasing $\delta^{13}C\text{-}CO_2$ indicates that rising ocean temperature contributed to the CO_2 rise with additional (but limited) changes in the net flux of organic carbon. This simplest of scenarios is somewhat surprising given that changes in the ocean's biological pump may accompany the large and abrupt reorganization of ocean circulation and changes in terrestrial carbon reservoirs are clearly indicted by

the large increases in CH_4 and N_2O (Figure 5e). More plausibly, yet more challenging to accurately model, are a roughly synchronous changes in several sources. Recently, the LOVECLIM model, which predicts a small positive relationship between CO_2 and $\delta^{13}C$-CO_2 during reduced NADW (Menviel et al., 2015), also predicts increases in CO_2 of 10 to 15 ppm upon the resumption of NADW(with the effect of solubility contributing about 50% to CO_2 variability)(Menviel et al., 2015). Moreover, a precisely dated coral record shows that these events during the last deglaciation are associated with brief intervals of enhanced overturning in the Atlantic (Chen et al., 2015). This integrated response to the onset of an interstadial is consistent with the CO_2 and $\delta^{13}C$-CO_2 data, and may be a pervasive feature of last glacial period CO_2 variability, but requires ground-truthing with additional, high-resolution MIS3 marine records.

Conclusions

Carbon isotope data from the last deglaciation and last glacial period clearly show that CO_2 variability is the sum of multiple mechanisms, many of which are triggered by abrupt climate change. During both periods millennial-scale variability is present and likely associated with the release of respired organic carbon from the deep ocean. Superimposed on these oscillations are two types of centennial-scale changes i) CO_2 increases and $\delta^{13}C$-CO_2 decreases in the middle of Heinrich stadials and ii) CO_2 increases and small changes in $\delta^{13}C$-CO_2 that are in-phase with rapid increases in NH temperature. During the deglaciation the millennial-scale component is enhanced and an additional carbon source is required to sustain the CO_2 rise through the entire deglaciation. This suggests that although abrupt climate variability is not the sole driver of the deglacial CO_2 rise, it may be a prerequisite. These potential links can now be tested with model experiments that use the MIS3 data to constrain the sensitivity to centennial and millennial-scale components and the deglacial data to evaluate how these mechanisms interact with changes in insolation, ice volume and global temperatures.

Acknowledgements

This work was funded by NSF grants ANT 0838936 (Oregon State University), ANT 0839031 (Scripps Institution of Oceanography). Data will be made available online at National Climate Data Center: https://www.ncdc.noaa.gov/paleo/study/24170

References

Ahn, J., & Brook, E. J. (2008). Atmospheric CO_2 and climate on millennial time scales during the last glacial period. *Science*, *322*(5898), 83–85. https://doi.org/10.1126/science.1160832

Ahn, J., & Brook, E. J. (2014). Siple Dome ice reveals two modes of millennial CO_2 change during the last ice age. *Nature Communications*, *5*, 3723.

Anderson, R. F., Ali, S., Bradtmiller, L. I., Nielsen, S. H. H., Fleisher, M. Q., Anderson, B. E., & Burckle, L. H. (2009). Wind-Driven Upwelling in the Southern Ocean and the Deglacial Rise in Atmospheric CO_2. *Science*, *323*(5920), 1443–1448. https://doi.org/10.1126/science.1167441

Anderson, R. F., Barker, S., Fleisher, M., Gersonde, R., Goldstein, S. L., Kuhn, G., et al. (2014). Biological response to millennial variability of dust and nutrient supply in the Subantarctic South Atlantic Ocean. *Philosophical Transactions of the Royal Society of London A: Mathematical, Physical and Engineering Sciences*, *372*(2019). https://doi.org/10.1098/rsta.2013.0054

Baggenstos, D., Bauska, T. K., Severinghaus, J. P., Lee, J. E., Schaefer, H., Buizert, C., et al. (2017). Atmospheric gas records from Taylor Glacier, Antarctica, reveal ancient ice with ages spanning the entire last glacial cycle. *Climate of the Past*, *13*(7), 943–958. https://doi.org/10.5194/cp-13-943-2017

Barker, S., & Diz, P. (2014). Timing of the descent into the last Ice Age determined by the bipolar seesaw. *Paleoceanography*, *29*(6), 489–507. https://doi.org/10.1002/2014PA002623

Bauska, T. K., Brook, E. J., Mix, A. C., & Ross, A. (2014). High-precision dual-inlet IRMS measurements of the stable isotopes of CO_2 and the N_2O / CO_2 ratio from polar ice core samples. *Atmos. Meas. Tech.*, *7*(11), 3825–3837. https://doi.org/10.5194/amt-7-3825-2014

Bauska, T. K., Joos, F., Mix, A. C., Roth, R., Ahn, J., & Brook, E. J. (2015). Links between atmospheric carbon dioxide, the land carbon reservoir and climate over the past millennium. *Nature Geoscience*, *8*, 383–387. https://doi.org/10.1038/ngeo2422

Bauska, T. K., Baggenstos, D., Brook, E. J., Mix, A. C., Marcott, S. A., Petrenko, V. V., et al. (2016). Carbon isotopes characterize rapid changes in atmospheric carbon dioxide during the last deglaciation. *Proceedings of the National Academy of Sciences*, *113*(13), 3465–3470. https://doi.org/10.1073/pnas.1513868113

354 Bereiter, B., Lüthi, D., Siegrist, M., Schüpbach, S., Stocker, T. F., & Fischer, H. (2012). Mode change of
355 millennial CO_2 variability during the last glacial cycle associated with a bipolar marine carbon
356 seesaw. *Proceedings of the National Academy of Sciences*, *109*(25), 9755–9760.
357 https://doi.org/10.1073/pnas.1204069109
358 Broecker, W. S., & McGee, D. (2013). The ^{13}C record for atmospheric CO_2: What is it trying to tell us?
359 *Earth and Planetary Science Letters*, *368*(0), 175–182.
360 https://doi.org/10.1016/j.epsl.2013.02.029
361 Brook, E. J., Harder, S., Severinghaus, J., Steig, E. J., & Sucher, C. M. (2000). On the origin and timing of
362 rapid changes in atmospheric methane during the last glacial period. *Global Biogeochemical*
363 *Cycles*, *14*(2), 559–572.
364 Buizert, C., Cuffey, K. M., Severinghaus, J. P., Baggenstos, D., Fudge, T. J., Steig, E. J., et al. (2015). The
365 WAIS Divide deep ice core WD2014 chronology – Part 1: Methane synchronization (68–31 ka
366 BP) and the gas age–ice age difference. *Clim. Past*, *11*(2), 153–173.
367 https://doi.org/10.5194/cp-11-153-2015
368 Charles, C. D., Lynch-Stieglitz, J., Ninnemann, U. S., & Fairbanks, R. G. (1996). Climate connections
369 between the hemisphere revealed by deep sea sediment core/ice core correlations. *Earth and*
370 *Planetary Science Letters*, *142*(1), 19–27. https://doi.org/10.1016/0012-821X(96)00083-0
371 Charles, C. D., Pahnke, K., Zahn, R., Mortyn, P. G., Ninnemann, U., & Hodell, D. A. (2010). Millennial scale
372 evolution of the Southern Ocean chemical divide. *Quaternary Science Reviews*, *29*(3–4), 399–
373 409. http://dx.doi.org/10.1016/j.quascirev.2009.09.021
374 Chen, T., Robinson, L. F., Burke, A., Southon, J., Spooner, P., Morris, P. J., & Ng, H. C. (2015). Synchronous
375 centennial abrupt events in the ocean and atmosphere during the last deglaciation. *Science*,
376 *349*(6255), 1537–1541. https://doi.org/10.1126/science.aac6159
377 Cheng, H., Edwards, R. L., Sinha, A., Spötl, C., Yi, L., Chen, S., et al. (2016). The Asian monsoon over the
378 past 640,000 years and ice age terminations. *Nature*, *534*, 640.
379 Clark, P. U., Shakun, J. D., Marcott, S. A., Mix, A. C., Eby, M., Kulp, S., et al. (2016). Consequences of
380 twenty-first-century policy for multi-millennial climate and sea-level change. *Nature Clim.*
381 *Change*, *6*(4), 360–369.

Eggleston, S., Schmitt, J., Bereiter, B., Schneider, R., & Fischer, H. (2016). Evolution of the stable carbon isotope composition of atmospheric CO_2 over the last glacial cycle. *Paleoceanography*, *31*(3), 434–452. https://doi.org/10.1002/2015PA002874

Ehleringer, J. R., Cerling, T. E., & Helliker, B. R. (1997). C4 photosynthesis, atmospheric CO_2, and climate. *Oecologia*, *112*(3), 285–299. https://doi.org/10.1007/s004420050311

Fischer, H., Fundel, F., Ruth, U., Twarloh, B., Wegner, A., Udisti, R., et al. (2007). Reconstruction of millennial changes in dust emission, transport and regional sea ice coverage using the deep {EPICA} ice cores from the Atlantic and Indian Ocean sector of Antarctica. *Earth and Planetary Science Letters*, *260*(1–2), 340–354. http://dx.doi.org/10.1016/j.epsl.2007.06.014

Gottschalk, J., Skinner, L. C., Lippold, J., Vogel, H., Frank, N., Jaccard, S. L., & Waelbroeck, C. (2016). Biological and physical controls in the Southern Ocean on past millennial-scale atmospheric CO_2 changes. *Nature Communications*, *7*, 11539.

Henry, L. G., McManus, J. F., Curry, W. B., Roberts, N. L., Piotrowski, A. M., & Keigwin, L. D. (2016). North Atlantic ocean circulation and abrupt climate change during the last glaciation. *Science*, *353*(6298), 470–474. https://doi.org/10.1126/science.aaf5529

Hodell, D. A., Kanfoush, S. L., Shemesh, A., Crosta, X., Charles, C. D., & Guilderson, T. P. (2001). Abrupt cooling of Antarctic surface waters and sea ice expansion in the South Atlantic sector of the Southern Ocean at 5000 cal yr B.P. *Quaternary Research*, *56*(2), 191–198.

Hodell, D. A., Venz, K. A., Charles, C. D., & Ninnemann, U. S. (2003). Pleistocene vertical carbon isotope and carbonate gradients in the South Atlantic sector of the Southern Ocean. *Geochemistry Geophysics Geosystems*, *4*. https://doi.org/10.1029/2002gc000367

Indermuhle, A., Wahlen, M. .. Monnin, E. .. Stauffer, B. .. Stocker, T. F. (2000). Atmospheric CO_2 concentration from 60 to 20 kyr BP from the Taylor Dome ice core, Antarctica. *Geophysical Research Letters*, *27*(5), 735–738.

Jaccard, S. L., Galbraith, E. D., Martínez-García, A., & Anderson, R. F. (2016). Covariation of deep Southern Ocean oxygenation and atmospheric CO2 through the last ice age. *Nature*, *530*, 207–210.

409 Kohler, P., Fischer, H., Schmitt, J., & Munhoven, G. (2006). On the application and interpretation of
410 Keeling plots in paleo climate research - deciphering delta C-13 of atmospheric CO_2 measured
411 in ice cores. *Biogeosciences*, *3*(4), 539–556.
412 Marcott, S. A., Bauska, T. K., Buizert, C., Steig, E. J., Rosen, J. L., Cuffey, K. M., et al. (2014). Centennial-
413 scale changes in the global carbon cycle during the last deglaciation. *Nature*, *514*(7524), 616–
414 619.
415 Martínez-García, A., Sigman, D. M., Ren, H., Anderson, R. F., Straub, M., Hodell, D. A., et al. (2014). Iron
416 Fertilization of the Subantarctic Ocean During the Last Ice Age. *Science*, *343*(6177), 1347.
417 https://doi.org/10.1126/science.1246848
418 McManus, J. F., Francois, R., Gherardi, J. M., Keigwin, L. D., & Brown-Leger, S. (2004). Collapse and rapid
419 resumption of Atlantic meridional circulation linked to deglacial climate changes. *Nature*,
420 *428*(6985), 834–837. https://doi.org/10.1038/nature02494
421 Menviel, L., Joos, F., & Ritz, S. P. (2012). Simulating atmospheric CO_2, ^{13}C and the marine carbon cycle
422 during the Last Glacial–Interglacial cycle: possible role for a deepening of the mean
423 remineralization depth and an increase in the oceanic nutrient inventory. *Quaternary Science*
424 *Reviews*, *56*, 46–68.
425 Menviel, L., Spence, P., & England, M. H. (2015). Contribution of enhanced Antarctic Bottom Water
426 formation to Antarctic warm events and millennial-scale atmospheric {CO_2} increase. *Earth*
427 *and Planetary Science Letters*, *413*, 37–50. http://dx.doi.org/10.1016/j.epsl.2014.12.050
428 Menviel, Laurie, Mouchet, A., Meissner, K., Joos, F., & England, M. (2015). Impact of oceanic circulation
429 changes on atmospheric $\delta^{13}CO_2$. *Global Biogeochemical Cycles*, *29*(11), 1944–1961.
430 North Greenland Ice Core Project Members. (2004). High-resolution record of Northern Hemisphere
431 climate extending into the last interglacial period. *Nature*, *431*(7005), 147–151.
432 Ninnemann, U. S., Charles, C. D., & Hodell, D. A. (1999). Origin of Global Millennial Scale Climate Events:
433 Constraints from the Southern Ocean Deep Sea Sedimentary Record. In *Mechanisms of Global*
434 *Climate Change at Millennial Time Scales* (pp. 99–112). American Geophysical Union.
435 https://doi.org/10.1029/GM112p0099

Rhodes, R. H., Brook, E. J., Chiang, J. C. H., Blunier, T., Maselli, O. J., McConnell, J. R., et al. (2015). Enhanced tropical methane production in response to iceberg discharge in the North Atlantic. *Science*, *348*(6238), 1016–1019. https://doi.org/10.1126/science.1262005

Schilt, A., Baumgartner, M., Schwander, J., Buiron, D., Capron, E., Chappellaz, J., et al. (2010). Atmospheric nitrous oxide during the last 140,000 years. *Earth and Planetary Science Letters*, *300*(1–2), 33–43. https://doi.org/10.1016/j.epsl.2010.09.027

Schilt, Adrian, Brook, E. J., Bauska, T. K., Baggenstos, D., Fischer, H., Joos, F., et al. (2014). Isotopic constraints on marine and terrestrial N_2O emissions during the last deglaciation. *Nature*, *516*(7530), 234–237.

Schmitt, J., Schneider, R., Elsig, J., Leuenberger, D., Lourantou, A., Chappellaz, J., et al. (2012). Carbon Isotope Constraints on the Deglacial CO_2 Rise from Ice Cores. *Science*, *336*(6082), 711–714. https://doi.org/10.1126/science.1217161

Schmittner, A., & Lund, D. C. (2015). Early deglacial Atlantic overturning decline and its role in atmospheric CO_2 rise inferred from carbon isotopes ($\delta^{13}C$). *Clim. Past*, *11*(2), 135–152. https://doi.org/10.5194/cp-11-135-2015

Seltzer, A. M., Buizert, C., Baggenstos, D., Brook, E. J., Ahn, J., Yang, J.-W., & Severinghaus, J. P. (2017). Does $\delta^{18}O$ of O_2 record meridional shifts in tropical rainfall? *Climate of the Past*, *13*(10), 1323–1338. https://doi.org/10.5194/cp-13-1323-2017

Severinghaus, J. P., Beaudette, R., Headly, M. A., Taylor, K., & Brook, E. J. (2009). Oxygen-18 of O_2 Records the Impact of Abrupt Climate Change on the Terrestrial Biosphere. *Science*, *324*(5933), 1431–1434. https://doi.org/10.1126/science.1169473

Sigman, D. M., Hain, M. P., & Haug, G. H. (2010). The polar ocean and glacial cycles in atmospheric CO_2 concentration. *Nature*, *466*(7302), 47–55. https://doi.org/10.1038/nature09149

Skinner, L. C., Fallon, S., Waelbroeck, C., Michel, E., & Barker, S. (2010). Ventilation of the Deep Southern Ocean and Deglacial CO_2 Rise. *Science*, *328*(5982), 1147–1151. https://doi.org/10.1126/science.1183627

462 Tschumi, T., Joos, F., Gehlen, M., & Heinze, C. (2011). Deep ocean ventilation, carbon isotopes, marine
463 sedimentation and the deglacial CO_2 rise. *Climate of the Past*, *7*(3), 771–800.
464 https://doi.org/10.5194/cp-7-771-2011
465 WAIS Divide Project Members. (2015). Precise interpolar phasing of abrupt climate change during the
466 last ice age. *Nature*, *520*(7549), 661–665.
467 Ziegler, M., Diz, P., Hall, I. R., & Zahn, R. (2013). Millennial-scale changes in atmospheric CO_2 levels
468 linked to the Southern Ocean carbon isotope gradient and dust flux. *Nature Geosci*, *6*(6), 457–
469 461.
470

Figure 1

Taylor Glacier CO_2, CH_4, N_2O and $\delta^{13}C\text{-}CO_2$ (blue markers with black smoothing spline, *this study*). Panel A: NGRIP $\delta^{18}O$(North Greenland Ice Core Project Members, 2004). B: WDC $\delta^{18}O$(WAIS Divide Project Members, 2015). C: Hulu Cave $\delta^{18}O$ (Cheng et al., 2016) D: WDC (Rhodes et al., 2015) (thin black line) and Taylor Glacier CH_4. E: Siple Dome (Ahn & Brook, 2014)(gray markers) and Taylor Glacier CO_2. F: Taylor Glacier $\delta^{13}C\text{-}CO_2$. G: Talos Dome (Schilt et al., 2010) (gray markers) and Taylor Glacier N_2O. H: Global Terrestrial O_2 isotopic fractionation, $\Delta\varepsilon_{LAND,}$ constrained from a combination of WDC and Siple Dome (Seltzer et al., 2017; Severinghaus et al., 2009). Dotted lines highlight the stadial to interstadial transitions and the red bar highlights the Heinrich Stadial with the associated rise in CO_2, CH_4 and increase in $\Delta\varepsilon_{LAND}$. The NGRIP chronology is increased by 0.63% prior to 22ka for consistency with the WDC chronology (WAIS Divide Project Members, 2015).

Figure 2

Cross-plot of atmospheric CO_2 and $\delta^{13}C\text{-}CO_2$ spanning the MIS3 section (blue, this study) and the last deglaciation, which is subdivide into the LGM to HS1 data (red) and late-Deglaciation (gray). Solid lines indicate linear regressions through the MIS3 (blue) and HS1 (red) data.

Figure 3

Comparison of atmospheric record of $\delta^{13}C\text{-}CO_2$ with oceanic records of $\delta^{13}C$ and nutrient utilization. A: Atmospheric $\delta^{13}C\text{-}CO_2$ (this study) on an inverted y-axis. B: The difference in $\delta^{13}C$ between Sub-Antarctic mode water (SAMW) and circumpolar deepwater (CDW)(Ziegler et al., 2013). A stack of benthic $\delta^{13}C$ (black line) from a combination of record in the deep Southern Ocean (grey circles) (Charles et al., 1996; Hodell et al., 2001, 2003; Ninnemann et al., 1999). Also indicated is the uncertainty on these chronologies (Barker & Diz 2014) based on synchronization between carbonate preservation and Greenland temperature (black boxes) and independent age control based on the Laschamp event (blue boxes). D: Foraminfera-bound $\delta^{15}N$ indicating nitrate consumption in Subantarctic (Martínez-García et al., 2014). Red bars highlight the broad millennia-scale correlations.

Figure 4

Left Panel: Comparison of MIS3 data *(this study)* and Last Deglaciation (Bauska et al., 2016; Marcott et al., 2014; Rhodes et al., 2015) greenhouse gas variability. A: WDC CH_4 (Rhodes et al., 2015). B: Taylor Glacier N_2O. C: Taylor Glacier CO_2. D: Taylor Glacier $\delta^{13}C\text{-}CO_2$. E: Pa/Th, a proxy for the strength of NADW formation (Henry et al., 2016; McManus et al., 2004)(orange), F: the opal flux in the SO(Anderson et al., 2009), a proxy for upwelling (green) (note the two different cores and axes are used in the comparison), G: the benthic to atmosphere ^{14}C age reconstructions for the Subantarctic zone(Gottschalk et al., 2016; Skinner et al., 2010), H: nssCa flux from the EDML ice core(Fischer et al., 2007), a proxy for dust delivery to Antarctica (brown), I: opal flux in the Subantarctic zone(Gottschalk

et al., 2016), a proxy for productivity (from the same core as the ventilation reconstruction). Yellow bars highlight the onset of interstadial conditions, black bars indicted the initial CO_2 rises and red bars correspond to the rapid jumps in CO_2 and CH_4. Right Panel: Centennial-scale variability during the last glacial period from Taylor Glacier and WAIS Divide. Anomalies in the concentration and isotopic composition of the greenhouse gases are plotted with the relative timing determined by the mid-point in the CH_4 rise. Marker color corresponds to dashed lines in left panel.

Figure 1.

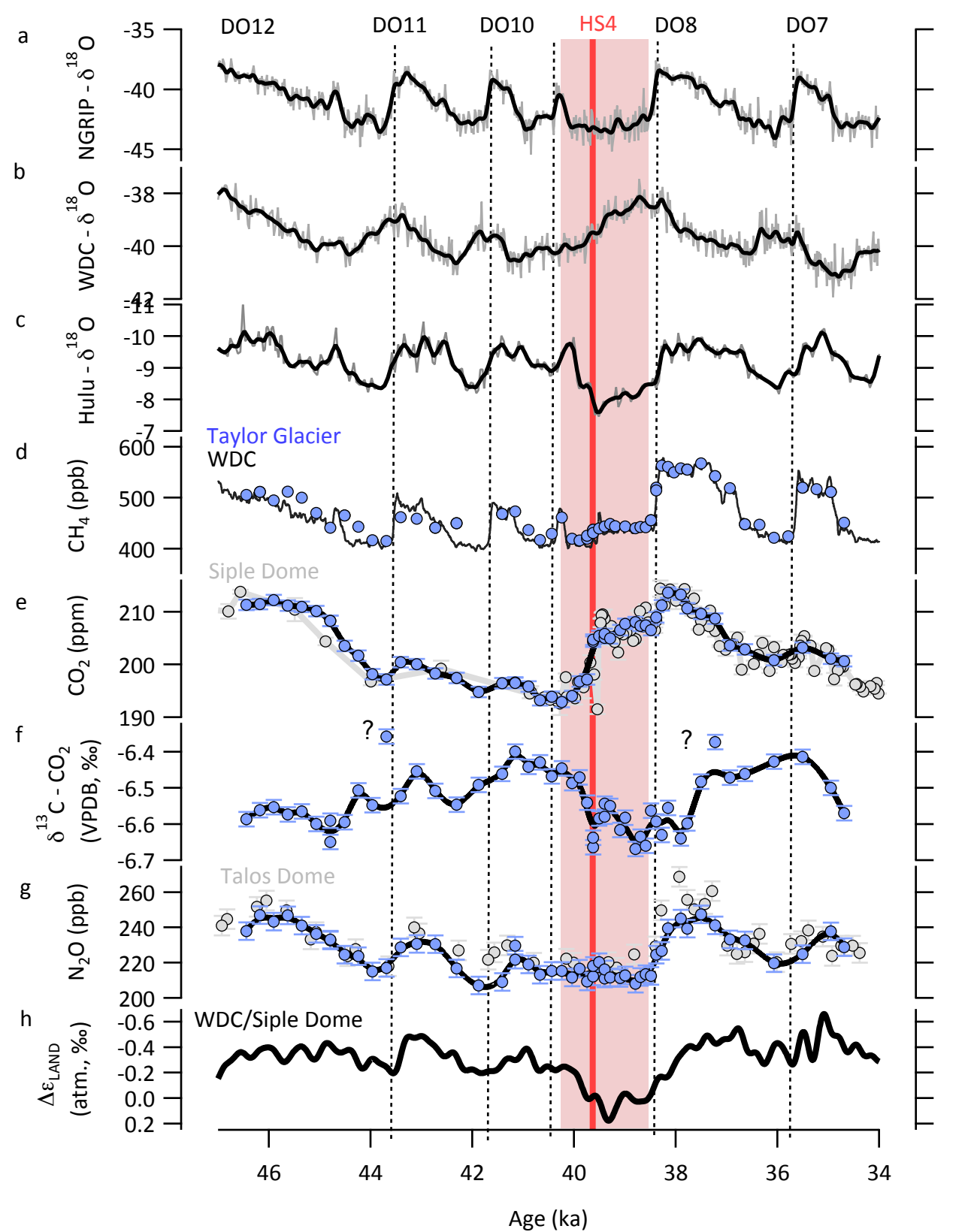
a
NGRIP - δ18O
-35
-40
-45
DO12
DO11
DO10
HS4
DO8
DO7
b
WDC - δ18O
-38
-40
-42
c
Hulu - δ18O
-10
-9
-8
-7
d
CH4 (ppb)
600
500
400
Taylor Glacier
WDC
e
CO2 (ppm)
210
200
190
Siple Dome
f
δ13C - CO2 (VPDB, ‰)
-6.4
-6.5
-6.6
-6.7
?
?
g
N2O (ppb)
260
240
220
200
Talos Dome
h
ΔεLAND (atm., ‰)
-0.6
-0.4
-0.2
0.0
0.2
WDC/Siple Dome
46
44
42
40
38
36
34
Age (ka)

Figure 2.

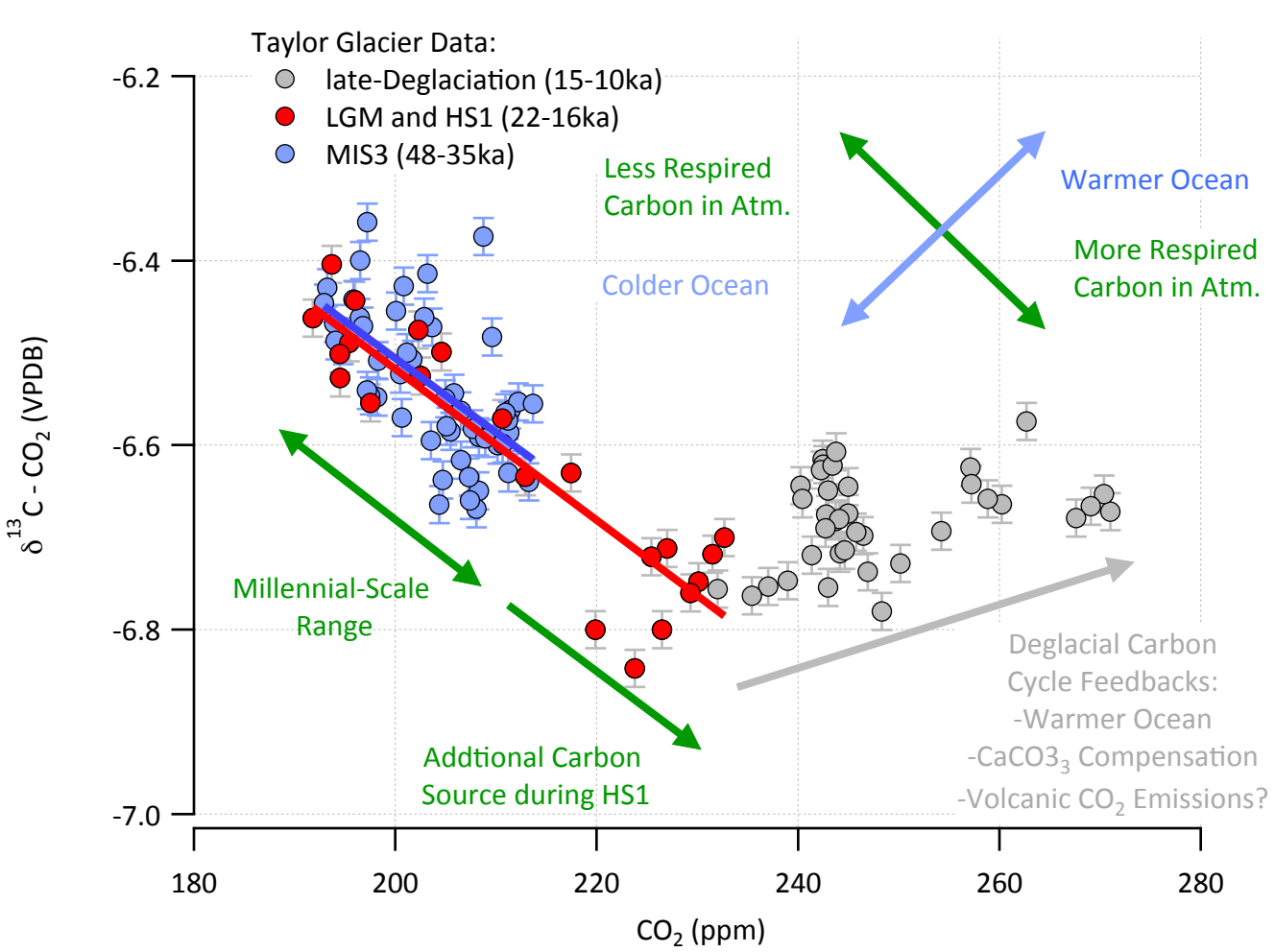
Taylor Glacier Data:
late-Deglaciation (15-10ka)
LGM and HS1 (22-16ka)
MIS3 (48-35ka)
Less Respired Carbon in Atm.
Colder Ocean
Warmer Ocean
More Respired Carbon in Atm.
Millennial-Scale Range
Addtional Carbon Source during HS1
Deglacial Carbon Cycle Feedbacks:
-Warmer Ocean
-CaCO3 Compensation
-Volcanic CO2 Emissions?
δ13C - CO2 (VPDB)
CO2 (ppm)
-6.2
-6.4
-6.6
-6.8
-7.0
180
200
220
240
260
280

Figure 3.

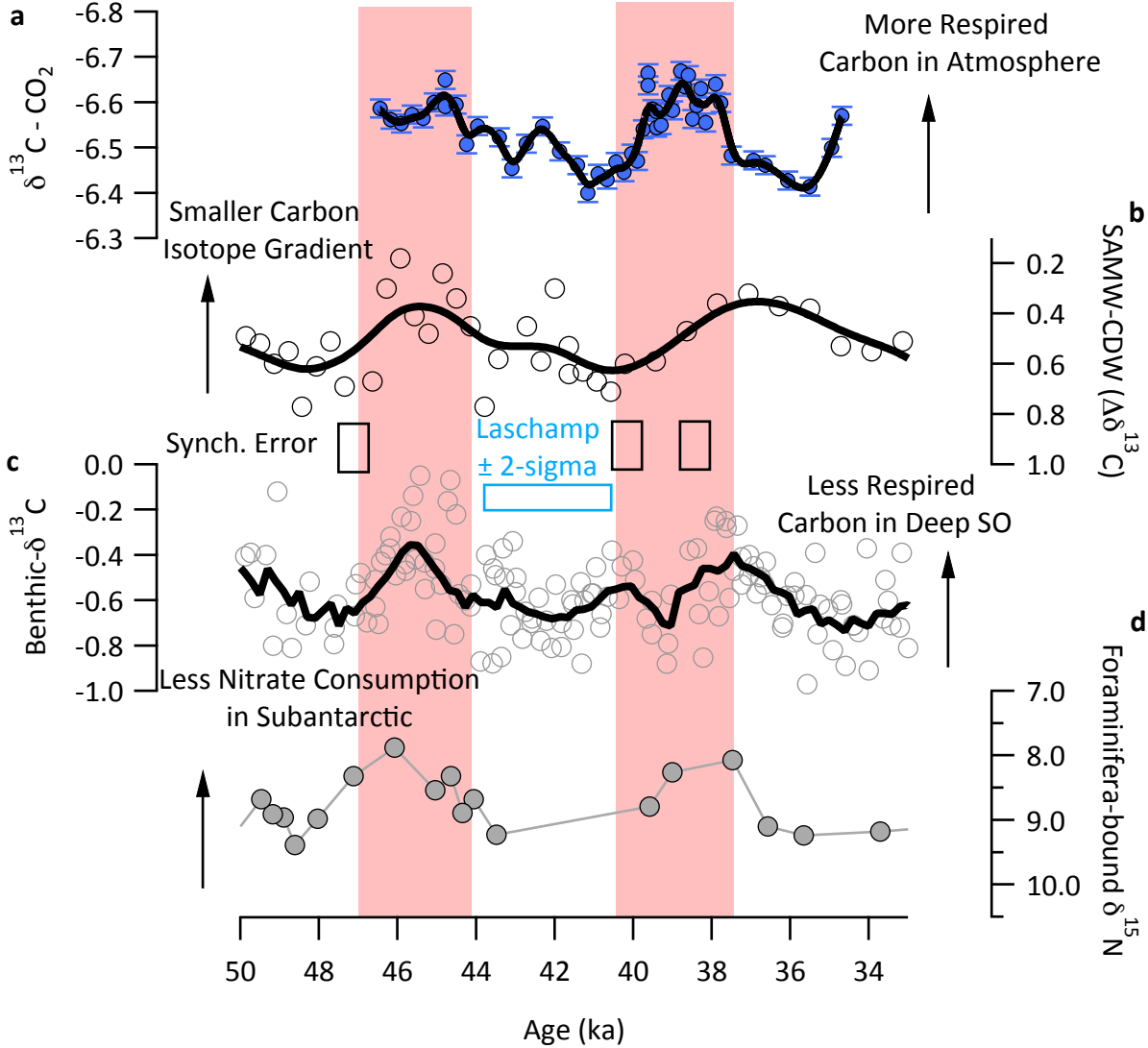
a
-6.8
-6.7
-6.6
-6.5
-6.4
-6.3
δ13C - CO2
More Respired
Carbon in Atmosphere
Smaller Carbon
Isotope Gradient
b
0.2
0.4
0.6
0.8
1.0
SAMW-CDW (Δδ13C)
Synch. Error
Laschamp
± 2-sigma
c
0.0
-0.2
-0.4
-0.6
-0.8
-1.0
Benthic-δ13C
Less Respired
Carbon in Deep SO
Less Nitrate Consumption
in Subantarctic
d
7.0
8.0
9.0
10.0
Foraminifera-bound δ15N
50
48
46
44
42
40
38
36
34
Age (ka)

Figure 4.

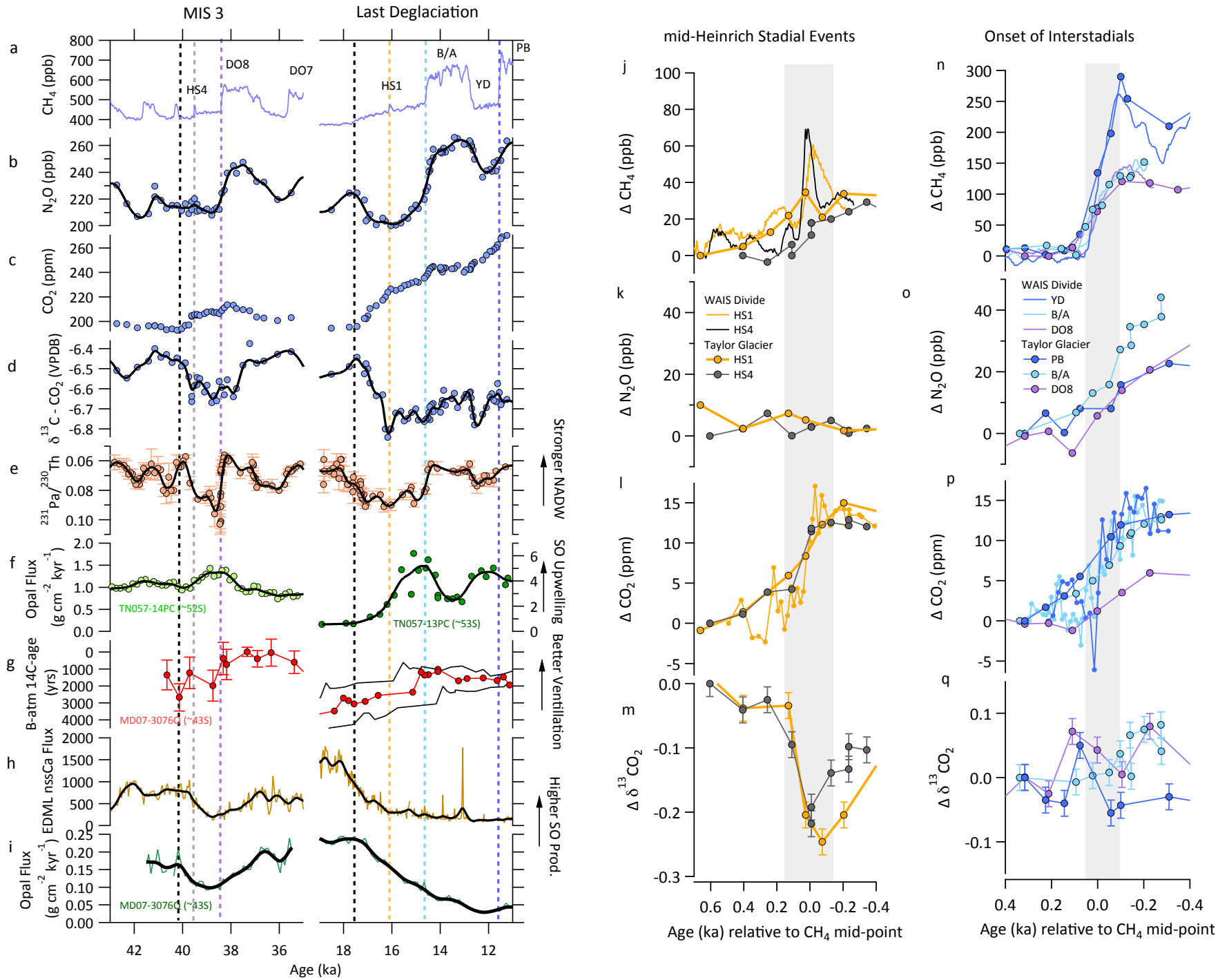
MIS 3
Last Deglaciation
mid-Heinrich Stadial Events
Onset of Interstadials
HS4
DO8
DO7
HS1
B/A
YD
PB
CH4 (ppb)
N2O (ppb)
CO2 (ppm)
δ13C - CO2 (VPDB)
231Pa/230Th
Opal Flux (g cm-2 kyr-1)
TN057-14PC (~52S)
TN057-13PC (~53S)
B-atm 14C-age (yrs)
MD07-3076Q (~43S)
EDML nssCa Flux
Opal Flux (g cm-2 kyr-1)
MD07-3076Q (~43S)
Stronger NADW
SO Upwelling
Better Ventilation
Higher SO Prod.
Age (ka)
Δ CH4 (ppb)
Δ N2O (ppb)
Δ CO2 (ppm)
Δ δ13CO2
WAIS Divide
HS1
HS4
Taylor Glacier
HS1
HS4
WAIS Divide
YD
B/A
DO8
Taylor Glacier
PB
B/A
DO8
Age (ka) relative to CH4 mid-point
Age (ka) relative to CH4 mid-point